

Mapping Point Defects of Brookite TiO₂ for Photocatalytic Activity Beyond Anatase and P25

Sovann Khan, Minyeong Je, Donghun Kim, Seungwoo Lee, So-Hye Cho,* Taeseup Song,* and Heechae Choi*



Cite This: <https://dx.doi.org/10.1021/acs.jpcc.0c02091>



Read Online

ACCESS |



Metrics & More

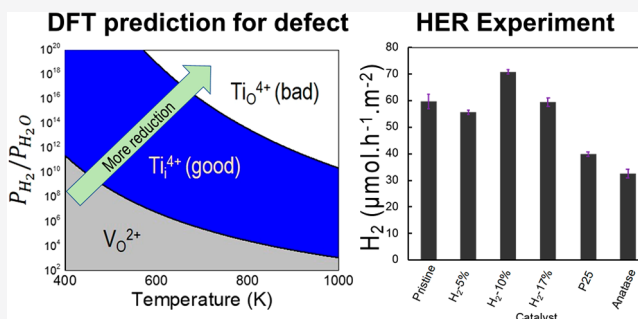


Article Recommendations



Supporting Information

ABSTRACT: Brookite, the least studied crystalline phase of TiO₂, recently has been found to have excellent photocatalytic activities, comparable to that of anatase TiO₂. However, its activity is highly dependent on its defect levels. We systematically studied the equilibria of the native point defects of brookite, along with their effects on photocatalytic activities. From first-principles calculations and thermodynamics modeling, we predicted the formation of an interstitial defect (Ti_i⁴⁺) under weak reductive conditions while that of Ti_o⁴⁺ under strong reductive conditions. Our calculations also suggest that Ti_i⁴⁺ exclusively induces ideal shallow defect levels in brookite, but Ti_o⁴⁺ results in deep level formations. In our experiments, we demonstrated that the moderately reduced brookite TiO₂ sample has the best photocatalytic activity. This combined theoretical and experimental work explains the inconsistent photocatalytic activities of brookite and suggests the processing conditions that yield highly active brookite photocatalysts—one that is comparable to or exceeding that of anatase.



INTRODUCTION

Natural crystalline TiO₂ has three main forms: rutile, anatase, and brookite.^{1–3} Among them, anatase and rutile have drawn the most attention because of their photoelectrical properties, making them applicable to photovoltaics or photocatalysis.^{3,4} On the other hand, brookite has seldom been utilized for such applications because of difficulties with its synthesis in a pure form.⁵ However, thanks to the development of several successful methods such as solvothermal, acidic oxidation, and hydrolysis/thermolysis,⁵ pure brookite is now commercially available. This development has allowed studies to explore the application of brookite, and several studies have even reported that its photocatalytic activity is comparable to anatase, the most widely applied crystalline phase for photocatalysis. However, unlike anatase, the physicochemical properties of brookite are not fully understood, and this has been hampering its development and usage.

In many cases, the qualities of photocatalysts largely rely on their defect levels when the same particle morphologies (e.g., size, shape, and facet) are considered. Because defects can alter the physicochemical properties of materials (e.g., band gaps, photoabsorption, redox levels, and carrier lifetimes), they have a significant influence on photocatalytic activity.^{2,6–8} Consequently, a large number of research has been devoted to studying the relationship between photocatalytic activities and the defects of the anatase phase.

For the fine engineering of defects on a semiconductor, the calculation of exact values of the defect formation energies and the defect levels is often quite useful.^{2,6,7,9,10} Density functional theory (DFT) calculations¹¹ have been successful in investigating the defect equilibria and related electronic structures of many oxide semiconductors, including that of anatase and rutile crystals.^{2,7,12} However, such studies, typically on defect studies combined experimental and computational works, have not intensively investigated on brookite thus far.^{12–14}

In this study, we systematically investigated the thermodynamic equilibria of point defects and electronic structures of pristine and defective brookite generated under different oxygen chemical potentials. Because the formation of shallow levels determines the photocatalytic activity of a material, accurate calculations of the electronic structures were necessary for this study. We used a hybrid-functional (HSE06)¹⁵ to obtain the values of the band gaps of pristine and defective brookite. Additionally, using DFT thermodynamics calculations as our guide, we demonstrated the impacts

Received: March 9, 2020

Revised: April 17, 2020

Published: April 20, 2020

of shallow level defects on photocatalytic activity enhancements.

We confirmed our predicted point defects with commercial brookite after post-treatment under different conditions. Also, we were able to prove our prediction regarding the relationship between brookite's defects and their photocatalytic activities by experimental verification: photocatalytic dye degradation and H₂ evolution.

Given the continuous interest in brookite's capabilities, and the lack of any comprehensive understanding of its properties, we provide an insight into the importance of successfully tailoring its defect chemistry to properly evaluate its photocatalytic activity.

CALCULATION METHODS

DFT calculations were performed using the generalized gradient approximation with Perdew–Burke–Ernzerhof (PBE) parameterization.^{16,17} We used the Vienna ab initio simulation package (VASP) program.¹⁸ Kohn–Sham orbitals were expanded with a cutoff energy of 400.0 eV, and 2 × 2 × 2 spaced *k*-point grids were employed for the Brillouin zone sampling in the electronic structure calculations.¹⁷ For our HSE06 calculations, a consistent screening parameter of $\mu = 0.2 \text{ \AA}^{-1}$ was used for the semilocal exchange and the screened nonlocal exchange. We used a mixture of 25% Hartree–Fock exchange with 75% PBE exchange to obtain the accurate band gaps of anatase.

The formation energy of the anatase ($\Delta E_{\text{TiO}_2}^f$) was obtained using the equation

$$\Delta E_{\text{TiO}_2}^f = E_{\text{TiO}_2} - E_{\text{Ti}} - E_{\text{O}_2} \quad (1)$$

where E_{TiO_2} , E_{Ti} , and E_{O_2} are the calculated total energies of the anatase crystal, solid Ti, and O₂ gas molecule, respectively. The calculated $\Delta E_{\text{TiO}_2}^f$ using the PBE method is -9.08 eV/f.u. , which only marginally differs from the experimental value (-9.11 eV/f.u.).¹⁸ Therefore, we regard the point defect formation energies obtained from the PBE calculations as substantial predictors of the dominant point defects.

To calculate the native defect formation energies of brookite for varying temperatures and pressures, the oxygen chemical potentials at a given temperature (*T*) and oxygen partial pressure (P_{O_2}) were expressed using the ideal gas approximation¹⁹

$$\mu_{\text{O}}(T, P_{\text{O}_2}) = \frac{1}{2} \left\{ \tilde{\mu}_{\text{O}_2}(T, P^\circ) + k_{\text{B}}T \ln \left(\frac{P_{\text{O}_2}}{P^\circ} \right) \right\} 20 \quad (2)$$

where $\tilde{\mu}_{\text{O}_2}(T, P^\circ)$ is the O₂ and chemical potential at temperature *T* and standard pressure (P°)¹⁷

The chemical potential of O is derived by

$$\frac{1}{2} \Delta E_{\text{TiO}_2}^f < \mu_{\text{O}} \leq 0 \quad (3)$$

where $\Delta E_{\text{TiO}_2}^f$ is the calculated heat of the formation of the brookite formula unit (10.61 eV). Defect formation energy with a charge *q* ($\Delta E^f(q)$), as a function of the Fermi level, can be calculated using the equation^{21,22}

$$\Delta E^f(q) = E[D^q] \pm \mu_i - E^0 + q(E_{\text{v}} + \Delta V + \epsilon_{\text{F}}) \quad (4)$$

where $E[D^q]$ is the total energy of the TiO₂ supercell with defects in a charge *q*; E^0 is the total energy of the defect-free TiO₂; μ_i is the chemical potential of the element *i* added to the supercell to generate a point defect; and E_{v} is the valence band maximum (VBM) of the defect-free TiO₂. Lastly, ΔV is the shift in the VBM of the defective cell by a point defect relative to that in the defect-free brookite, and ϵ_{F} is the Fermi level referenced to E_{v} .

The HSE06 method can provide accurate band gap values and defect formation energies. However, due to high computation cost, we employed an economical and quite reliable alternative method: extrapolation with the PBE and PBE + *U* method.^{13,23} The calculated band gap of anatase TiO₂ using PBE and PBE + *U* were 2.12 and 2.91 eV, respectively. Because the Hubbard *U*, however, does not fully correct the band gap (the experimental value is 3.2 eV) and the transition point of a defect charge, we extrapolated the transition point of a defect charge using the following eq 13¹³

$$\epsilon(q/q') = \epsilon(q/q')^{\text{PBE}+U} + \frac{\Delta \epsilon}{\Delta E_{\text{g}}} (E_{\text{g}}^{\text{exp}} - E_{\text{g}}^{\text{PBE}+U}) \quad (5)$$

with

$$\frac{\Delta \epsilon}{\Delta E_{\text{g}}} = \left(\frac{\epsilon(q/q')^{\text{PBE}+U} - \epsilon(q/q')^{\text{PBE}}}{E_{\text{g}}^{\text{PBE}+U} - E_{\text{g}}^{\text{PBE}}} \right) \quad (6)$$

where $\epsilon(q/q')$ is the transition point from charge *q* to *q'*. $E_{\text{g}}^{\text{exp}}$, $E_{\text{g}}^{\text{PBE}+U}$, and $E_{\text{g}}^{\text{PBE}}$ are the band gap energies obtained from the experiment, PBE + *U* and PBE calculations.

EXPERIMENTAL METHODS

Brookite nanoparticles were purchased from Sigma-Aldrich, USA (product no. 791326, size: <100 nm) and used after heat treatment at 500 °C for 10 min in the air (designated “pristine” in the text). The defects were induced by thermal annealing at 500 °C for 10 min. The various reductive environments were created by adjusting the H₂ concentrations in the H₂ and N₂ gas mixture (see Table 1), which is a quite common and safe

Table 1. Descriptions of Brookite Annealed at 500 °C (773 K) with Different Environment Conditions

sample	pristine	H ₂ -5%	H ₂ -7%	H ₂ -10%	H ₂ -13%	H ₂ -17%
H ₂ :N ₂		1:19	1:13	1:9	1:7	1:5

way to control the partial pressure of H₂.²⁴ We ruled out the possibility of ammonia (NH₃) formation by a thermal reaction of H₂ and N₂ because this reaction does not occur at 500 °C unless an extremely high pressure or a reactive catalyst is applied.²⁵

To compare photocatalytic activities, Anatase-TiO₂ (product no. 637254, size: <25 nm) and Aeroxide P25-TiO₂ (product no. 718467, size: ~21 nm) were purchased from Sigma-Aldrich, USA and used in the conditions they were received in. Along with them, methylene blue (MB) dissolved in an aqueous solution, and H₂PtCl₆ were likewise purchased from the same company.

The UV–vis absorption spectra were obtained by using the Jasco v-670 spectrophotometer (190–2700 nm), and the crystal structure was studied by X-ray diffraction (XRD; D8 Advanced, Bruker Corporation, USA). X-ray absorption near edge structures (XANES) and extended X-ray absorption fine

(EXAFS) data were collected from the lab-source X-ray absorption spectrometer (Rigaku; R-XAS) using a 3 kW X-ray generator with a W–W target–filament combination. The electron paramagnetic resonance (EPR) was analyzed by CW-EPR, QM09 (microwave frequency and power of 9.64 GHz and 4.6 mW, respectively, and modulation frequency of 100 kHz).

The photocatalytic activities of TiO₂ samples were determined by the MB degradation under UV light. TiO₂ powder (20 mg) was dispersed into 50 mL of MB (5 × 10^{−4} wt %) and placed under UV light (UV-B lamp, G15T8E, Sankyo Denki). After a predetermined time, a portion of the irradiated mixture solution was taken for centrifugation (13,500 rpm for 15 min) for the TiO₂ removal. The amount of remaining MB after the photocatalytic degradation was measured by UV–vis absorption at λ_{max} = 664 nm.^{7,23}

For the photocatalytic H₂ evolution reaction, a Pt-loading on TiO₂ particles was performed following Yu et al.'s work.²⁶ TiO₂ (30 mg) and H₂PtCl₆ (0.6 mg, 2 wt % to TiO₂) were dispersed into 15 mL of deionized water by stirring for 60 min at room temperature. The mixture was then sonicated for 20 min, followed by exposure to UV radiation for another 20 min. Pt-loaded TiO₂ particles were separated from the solution by centrifugation and dried in an oven (70 °C) for 18 h. Photocatalytic H₂ production was performed through a batch type reaction. Eight milligrams of each catalyst was placed in a 9 mL quartz tube equipped with a silicone rubber and dispersed in a mixture of 4 mL of de-ionized water and 2 mL of ethanol. Then, the colloidal solution was bubbled with N₂ gas for 10 min to remove the air inside the tube and then placed under the UV light (UV-B lamp, G15T8E, Sankyo Denki, Japan). After a predetermined time, 8 μL of gas was taken by a gas-tight syringe and injected into the gas chromatograph (GC-6500 GC system, YL Instrument, S. Korea) to quantify the H₂ concentration. Three sets of the experiments were conducted, and the averaged values of H₂ production were calculated based on the calibration curves obtained with the reference H₂ gas (Figure 1).

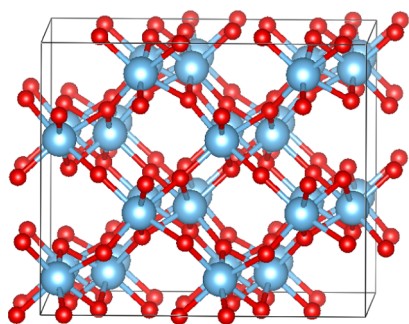


Figure 1. Supercell of 2 × 2 × 1 brookite.

RESULTS AND DISCUSSIONS

It has been long debated on whether charge carrier transport in TiO₂ crystals are bandlike or polaronic.²² In anatase, hole carrier transport is known to take a place mainly via polaron hopping, whereas electron transport occur by both bandlike and polaronic mechanism.^{27–29} So, we investigated the formation and hopping of polarons in brookite (Figure 2) to see if it could function similarly. Interestingly, we found that brookite can only generate electron polaron (Figure 2a);³⁰

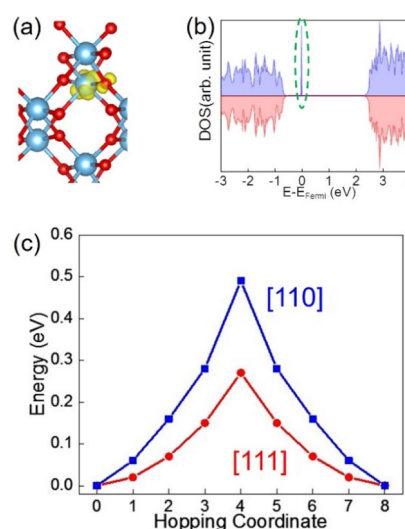


Figure 2. Calculated (a) spatial spin density isosurface; isovalue set at 0.02 e/Å³, (b) density of states, and (c) hopping energies of electron polaron.

where an extra electron polaron forms and self-traps at a Ti-site becoming Ti³⁺ instead of Ti⁴⁺. The trapped excess electron induces a sharp spin-polarized in-gap state (Figure 2b). With this localized excess of electrons, the Ti–O bond lengths are elongated by 3.5–6.0% compared to the neutral system.

The polaron mobility in semiconductors is generally modeled with the Marcus/Holstein theory as its framework—where a polaron hopping overcomes thermal activation barriers for transport. Thus, the formula of carrier mobility (μ) in the Marcus/Holstein theory is written as

$$\mu = \frac{eD}{k_B T} = \frac{e(1-c)a^2 v_0}{k_B T} \exp\left(-\frac{\Delta G}{k_B T}\right) \quad (7)$$

where D is the diffusion constant of carriers, $(1-c)$ is the probability that a neighboring site is available for hopping, ΔG is the activation energy barrier for polaron hopping, v_0 is the optical phonon frequency, and k_B is Boltzmann constant. The polaron hopping energy barriers were calculated by computing the system total energy changes at seven intermediate points in the path of hopping (Figure 2c). For polaron formations, Hubbard's U -term ($U = 6$ eV) on the Ti 3d orbital was included. We considered the hopping of electron polaron from one Ti-site to a neighboring Ti-site in the [110] and [111] directions, where the nearest Ti–Ti distances are 3.08 and 3.57 Å, respectively. The calculated thermal energy barriers, ΔG are 0.49 and 0.27 eV in the [110] and [111] directions, respectively. The calculated values of thermal energy barriers for electron polaron hopping in brookite are very close to those in anatase.²⁷ Therefore, any discrepancy in the photocatalytic activities of brookite and anatase is likely due to other factors, such as the optical phonon frequency, lifetime of carriers, and photoabsorption amounts.

The calculated formation energies of the native defects in brookite for the different conditions are illustrated in Figure 3. Because defect formation energy is determined as the pinned point of formation energy lines of positive and negative defects, the polaron formation energies need to be considered to suggest the dominant defects and their concentrations. For brookite, we calculated the electron and hole polaron formation energies with excess electrons and deficient electron,

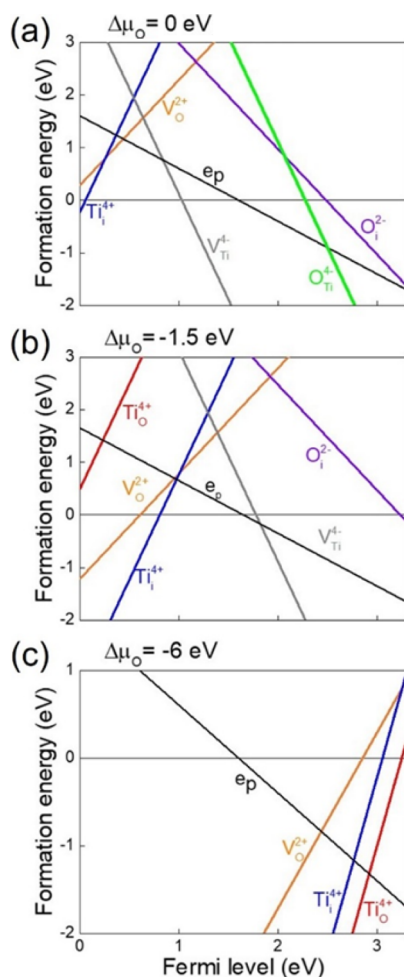


Figure 3. Calculated defect formation energies for (a) ambient conditions ($\Delta\mu_{\text{O}} = 0$ eV), (b) slightly reductive conditions ($\Delta\mu_{\text{O}} = -1.5$ eV), and (c) strongly reductive conditions ($\Delta\mu_{\text{O}} = -6$ eV).

respectively. To induce electron and hole polarons, we used Hubbard's U term²⁸ (effective $U = 6$ eV) with elongated bond lengths around a single Ti and O atom, respectively. Interestingly, the electron polaron was induced with lower energy than that of the excess electrons at a conduction band; all the while, hole polaron in brookite was not stably formed. Therefore, we considered only electron polaron formation in the defect chemistry of brookite.

In O-rich to ambient conditions ($\Delta\mu_{\text{O}} > -1.1$ eV), the dominant defect is the V_{O}^{2+} (Figure 3a). In slightly reductive conditions (-5.1 eV $< \Delta\mu_{\text{O}} < -1.1$ eV), the dominant defect changes to Ti_i^{4+} (Figure 3b). Then, further reducing conditions ($\Delta\mu_{\text{O}} < -5.1$ eV) results in the anti-site defect of Ti_o^{4+} to be dominant (Figure 3c). In consideration of our previous calculations on the point defects of anatase, where Ti_i^{4+} was found to dominate in wide oxidation conditions,⁷ point defects in brookite are more easily alterable. It may also explain why brookite has significantly varying photocatalytic activities depending on heat-treatment conditions.³¹

To investigate the energy levels of each defect, the electron density of states (DOS) of brookite supercells with various point defects were calculated (Figure 4). While the V_{O}^{2+} defect does not impose any notable change in the DOS of pristine brookite, the anti-site defect, Ti_o^{4+} , induces in-gap states at 0.6 eV below the CBM of pristine brookite. This can negatively

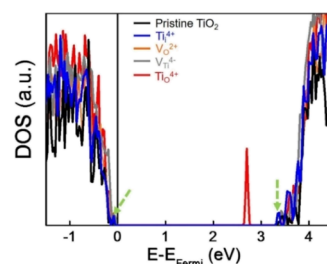


Figure 4. Calculated total electron DOS of the brookite supercell with various defects (black line = pristine brookite; blue = Ti_i^{4+} ; yellow = V_{O}^{2+} ; grey = $\text{V}_{\text{Ti}}^{4+}$; and red = Ti_o^{4+}).

affect its photocatalytic activity by increasing the electron–hole recombination rate.^{32,33} Unlike the Ti_i^{4+} defect in anatase supercells, which does not induce any in-gap states,⁷ in brookite supercells, it induces ideal shallow defect levels resulting in a band gap reduction of ~ 0.1 eV both at VBM and CBM (as noted by the green arrows in Figure 4). The shallow levels induced by Ti_i^{4+} in our calculation are consistent with the experimentally observed shallow impurity levels in Vequizo et al.'s report.³⁴

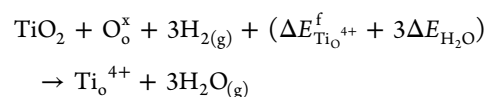
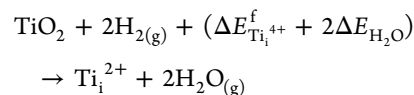
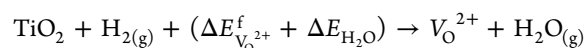
To generate Ti_i^{4+} defects in brookite and to induce ideal shallow levels, it is necessary to provide a moderate reductive condition (Figure 3). For an efficient reduction of TiO_2 , H_2 -assisted reductive annealing can be applied.^{1,35} In the reduction, H_2 gas can react with oxygen atoms in TiO_2 and form gaseous water (H_2O) molecules. The enthalpy of the $\text{H}_2\text{O}_{(\text{g})}$ formation from $1/2\text{O}_{2(\text{g})}$ and $\text{H}_{2(\text{g})}$ (-241.8 kJ/mol) can be the additional driving force of n-type point defect formations. Hence, we considered the hydrogen chemical potential (μ_{H_2}) as the parameter of simulating different reductive conditions. μ_{H_2} is expressed using the ideal gas approximation²⁹

$$\mu_{\text{H}_2}(T, P_{\text{H}_2}) = \left\{ \tilde{\mu}_{\text{H}_2}(T, P^\circ) + k_{\text{B}}T \ln\left(\frac{P_{\text{H}_2}}{P^\circ}\right) \right\} \quad (8)$$

where $\tilde{\mu}_{\text{H}_2}(T, P^\circ)$ is the H_2 chemical potential at a given temperature T and standard pressure P° . μ_{H} is the H chemical potential

$$\mu_{\text{H}} = \frac{1}{2}\mu_{\text{H}_2} \quad (9)$$

The reaction under each reductive condition can be drawn as



where $\Delta E_{\text{H}_2\text{O}}$ is the water formation energy from H_2 and O_2 . The formation energy differences are then expressed as

$$\Delta E_{\text{Ti}_i^{4+}}^f - \Delta E_{\text{V}_{\text{O}}^{2+}}^f = E[\text{Ti}_i^{4+}] - E[\text{V}_{\text{O}}^{2+}] - \mu_{\text{H}_2} + \mu_{\text{H}_2\text{O}} \quad (10)$$

$$\Delta E_{\text{Ti}_O^{4+}}^f - \Delta E_{\text{Ti}_i^{4+}}^f = E[\text{Ti}_O^{4+}] - E[\text{Ti}_i^{4+}] - \mu_{\text{H}_2} + \mu_{\text{H}_2\text{O}} \quad (11)$$

$E[\text{Ti}_O^{4+}]$ and $E[\text{Ti}_i^{4+}]$ are the calculated total energies of a brookite supercell with the Ti_O^{4+} and Ti_i^{4+} defects. Similar to hydrogen chemical potential (eq 8), the chemical potential of gaseous H_2O is given by

$$\mu_{\text{H}_2\text{O}}(T, P_{\text{H}_2\text{O}}) = \left\{ \tilde{\mu}_{\text{H}_2\text{O}}(T, P^\circ) + k_B T \ln \left(\frac{P_{\text{H}_2\text{O}}}{P^\circ} \right) \right\} \quad (12)$$

where $\tilde{\mu}_{\text{H}_2\text{O}}(T, P^\circ)$ is the chemical potential of H_2O at varying temperatures T and standard pressures (P°). Combining eqs 8 and 12, we rewrite eq 11 as

$$\begin{aligned} \Delta E_{\text{Ti}_O^{4+}}^f - \Delta E_{\text{Ti}_i^{4+}}^f &= E[\text{Ti}_O^{4+}] - E[\text{Ti}_i^{4+}] - \{ \tilde{\mu}_{\text{H}_2\text{O}}(T, P^\circ) \\ &\quad - \tilde{\mu}_{\text{H}_2}(T, P^\circ) \} + k_B T \ln \left(\frac{P_{\text{H}_2\text{O}}}{P_{\text{H}_2}} \right) \end{aligned} \quad (13)$$

Not only can eq 13 determine why the defect (between Ti_O^{4+} and Ti_i^{4+}) is dominant once conditions (T and P_{H_2}) are given, but it also informs of the condition needed for specific defects, which induce deteriorating deep levels and ideal shallow levels for strong photocatalysis.

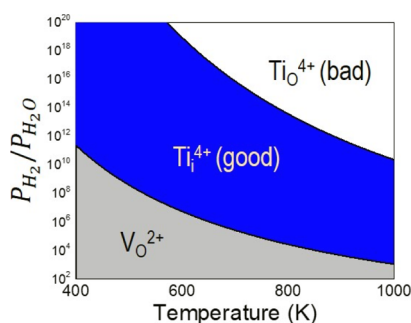


Figure 5. Defect diagram of brookite obtained from the calculated defect formation energies.

Figure 5 illustrates the calculated defect diagram obtained after using eqs 10, 11, and 13. In low temperature and low P_{H_2} region (grey area), V_O^{2+} is seen as the dominant defect. However, with increasing temperature or P_{H_2} (or decreasing P_{O_2}), the dominant defect is then predicted by the Ti_i^{4+} (blue) and Ti_O^{4+} (white) areas. By using the DOS calculations shown in Figure 4, we considered that the Ti_i^{4+} defect induces an expected shallow level ideal for the photocatalytic activity of brookite, whereas the Ti_O^{4+} defect degrades the activity by forming a deep level within the bandgap of brookite TiO_2 . Figure 5 suggests that to enhance the brookite's photocatalytic activity, reductions must be moderate.

To verify those theoretical predictions, we performed H_2 -assisted reductive annealing on commercially available brookite (<100 nm). We chose the annealing temperature of 500 °C (773 K) for a duration for 10 min because it is known that the brookite composition of TiO_2 transforms into rutile at high temperatures (e.g., >800 °C, if the brookite has high

crystallinity and phase purity) and that transformation temperature becomes even lower when defects are present.^{31,20,31} The reductive condition was generated by H_2 gas diluted in N_2 gas in different ratios. The annealing condition was engineered to be mild enough to preserve bulk powder properties, such as particle size and crystallinity. This was done because these properties can be dominant factors that determine the photocatalytic activity of TiO_2 , and we aimed to examine the role of surface defects. Table 1 summarizes the description of samples that are treated under different conditions.

The pristine sample changed color to tint grey after reductive annealing, while lower reductive conditions provided a lighter grey color, and higher reductive conditions resulted in a darker grey color (Figure S1). UV–vis absorption spectra of all samples showed strong absorptions in the UV range, which correspond well to the intrinsic band-gap of brookite (3.25 eV for indirect transition; 3.42 eV for direct transition⁵). Increased absorptions in the visible range were found for all reduced samples— H_2 -5% and H_2 -7% exhibit similar visible absorptions while H_2 -10%, H_2 -13%, and H_2 -17% show a gradual increase in absorptions along with increasing amounts of H_2 . The occurrence of extended absorptions to visible light by reductive annealing indicates the generation of electronic band tails by defect state formation, and the difference in visible absorptions by samples may infer the existence of multiple defect states. However, the similar levels of intrinsic UV absorptions by samples inform that the defective layer appears only within a certain depth from the outer surface of brookite particles (Figure 6).

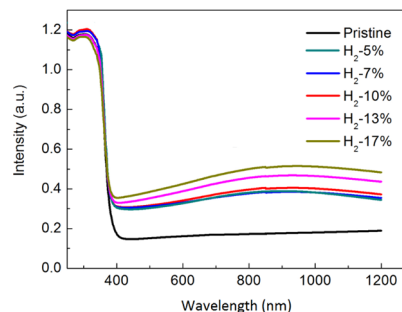


Figure 6. UV–vis absorption spectra of pristine and all reduced samples.

It is worth noting that analysis such as XRD patterns, scanning electron microscopy (SEM) and transmission electron microscopy (TEM) images, and Brunauer, Emmett, and Teller (BET) surface areas exhibited no substantial differences between pristine and reductively annealed samples (Figures S2 (SEM), S3 (TEM), S4 (XRD), and S5 (BET)). This assured us that the annealing condition was mild enough to retain the bulk properties of pristine TiO_2 .

XRD patterns, in particular, showed no signs of the other phases and little changes in peak intensity. According to previous research studies about brookite, it is quite difficult to obtain its pure crystalline form because crystallization by a mild sintering often results in phase transformation to anatase or rutile if the starting TiO_2 has amorphous or impure phases. Bakardjieva et al., for example, reported that nanometric brookite transforms to a mixed phase of brookite, anatase, and rutile at sintering temperatures as low as 200 °C.³⁶ The fact

that we did not observe the phase transformation under the relatively high annealing condition indicates that the pristine sample is in a crystalline state with high phase purity.

Next, we performed a slow-scanned XRD analysis on all samples in the range of 24–27° and found slight changes in lattice parameters and cell volumes by reductive annealing conditions (Figure S6; Table S1). In Figure 7, we depicted the

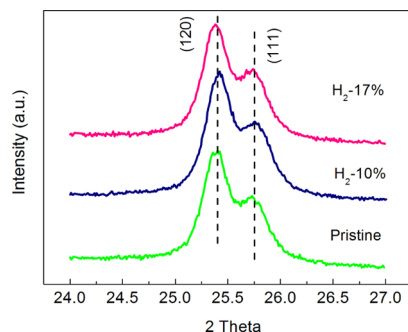


Figure 7. Slow-scanned XRD patterns at planes (120) and (111).

slow-scanned XRD spectra of only three samples, pristine, H₂-10%, and H₂-17% for better demonstration of changes. Diffraction peaks of plane [120] and [111] of H₂-10% slightly shifted to a higher angle than those of pristine, while those of H₂-17% showed a shift to a lower angle. These shifts of XRD peaks indicate changes in cell volumes. By comparing with the pristine sample, the volume of a unit cell of H₂-10% decreased by 0.45%, whereas that of H₂-17% increased by 0.53% (Table S1). The changes in cell volume demonstrate the induction of different defects by varying the H₂ during the thermal treatment.

Inspired by the XRD results, we examined the lattice disorders of the pristine, H₂-10% (moderately reduced), and H₂-17% (strongly reduced) samples with XANES/EXAFS measurement. From Ti K-edge XANES spectra, it was found that all three samples share similar spectral features which originate from the parent brookite structure (Figure S7). However, when local atomic structure was examined by Ti K-edge EXAFS data, changes in coordination numbers and atomic distances of Ti–O and Ti–Ti bonds were found. Figure 8 represents both Fourier transformed spectra of EXAFS data (black line) and theoretically fitted spectra (red line) of the pristine, H₂-10%, and H₂-17% samples. The sharp oscillation in 1.5–2.0 Å in the spectra is due to the first Ti–O shells, and the next two oscillations in 2.0–3.0 Å are due to the

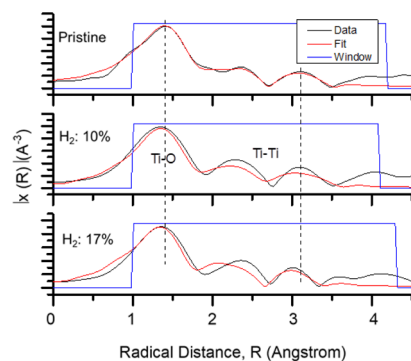


Figure 8. Radical distribution functions and their fitting curves for pristine, H₂-10%, and H₂-17%, obtained from Ti K-edge EXAFS data.

Ti–Ti shells. As indicated by the dotted lines in the figure, both Ti–O and Ti–Ti peaks of H₂-10% and H₂-17% show slight shifts to shorter distances compared to that of the pristine sample. Calculated distances of the Ti–Ti bond from these EXAFS spectra were 3.06, 3.02, and 2.99 Å for pristine, H₂-10%, and H₂-17%, respectively (Table 2). Moreover,

Table 2. Calculated Shell Parameters of Ti–O and Ti–Ti of pristine, H₂-10%, and H₂-17% by EXAFS Analysis

sample	shell	coordination no. (N)	bond distance (Å)
pristine	Ti–O	5.52	1.957
	Ti–Ti	3.60	3.069
H ₂ -10%	Ti–O	5.47	1.931
	Ti–Ti	4.94	3.021
H ₂ -17%	Ti–O	5.29	1.901
	Ti–Ti	5.32	2.994

calculated coordination numbers (*N*) also showed significant changes. The *N* for Ti–O decreased from 5.52 to 5.29, and for Ti–Ti, it increased from 3.60 to 5.32 when the *N* values of the pristine samples were compared to those of H₂-17% (Table 2). These results indicate that the volume of lattice disorder in brookite increases as more reductive conditions are applied. The defects, suggested by our DFT simulation of the reductively treated brookite, are Ti_i⁴⁺ and Ti_o⁴⁺, and occurrence of these defects can decrease both Ti–Ti bond length and the *N* of Ti–O but increase the *N* of the Ti–Ti shell. This agrees with our observation using EXAFS data. However, experimental deconvolution of contributions by each defect on the observed lattice disorder was not possible.

The photocatalytic activities of the samples listed above were then first evaluated by MB degradation reaction under UV light. By monitoring MB concentration decrease as a function of time (Figure 9a), it was found that the H₂-10% sample possesses distinctively higher activity than the pristine sample, while H₂-17% has slightly lower activity. This result indicates the presence of different surface defects across various reductive conditions because no bulk properties (i.e., size, shape, phase, and surface area) were changed by the treatment. When the decay constants (*k*) of MB by the reduced brookite samples were compared with those by commercial anatase and aerioxide P25 (anatase and rutile-mixed phase TiO₂), it was revealed that the activity of H₂-10% is comparable to that of P25 but superior to that of anatase (Figure 9b) when normalized by surface areas (Table S2). It should be noted that constants for P25 and anatase were normalized by their BET surface areas due to difference in their particle sizes. This study demonstrates that the photocatalytic activity of brookite can be manipulated by defect engineering to be comparable to that of P25, a well-known photocatalyst.

Considering our theoretical prediction on the possible defects and their role on the photocatalytic activity of brookite, we correlate the highest photocatalytic activity obtained at H₂-10% to the presence of Ti_i⁴⁺ defects by moderate reduction, while we correlate the sudden drop of photocatalytic activity at H₂-17% to the occurrence of Ti_o⁴⁺ defects. Many studies on reduced anatase argue that V_o²⁺ coupled with self-doped Ti³⁺ is the primary defect, and it is what forms an ideal shallow defect level below the CBM of anatase TiO₂; this affords the photocatalytic activity enhancement.^{37–39} We subsequently analyzed our samples in this respect. Three representative

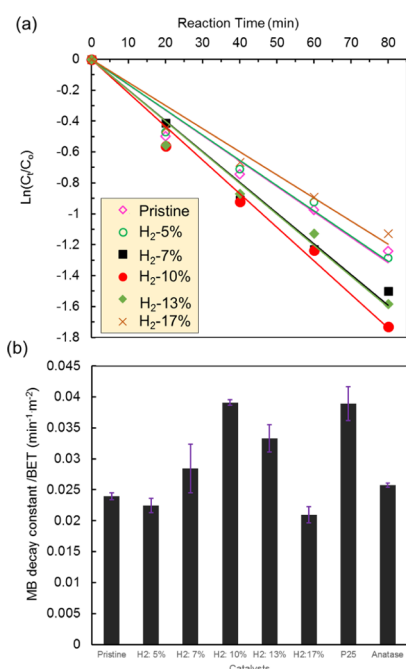


Figure 9. Photocatalytic degradation of MB by different TiO₂ samples under UV light: (a) natural logarithm plot of C_t/C_0 by a function of irradiation time (C_0 and C_t are initial MB concentration and MB concentration at irradiation time, t , respectively) and (b) decay constants of MB normalized per a surface area basis.

samples, pristine, H₂-10%, and H₂-17% were examined by X-ray photoelectron spectroscopy (XPS) and EPR (Figures S8 and 10). XPS analysis exhibited identical Ti 2p binding

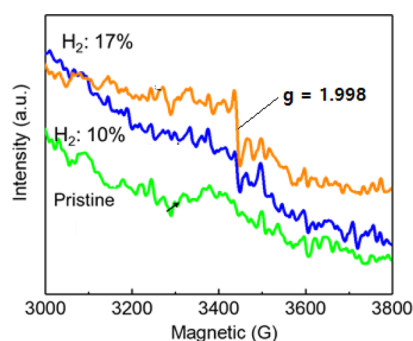


Figure 10. EPR spectra of pristine, H₂-10%, and H₂-17% samples.

energies of reduced samples (H₂-10% and H₂-17%) and pristine. However, it is known that binding energies of Ti³⁺ and Ti⁴⁺ are superposed so that XPS data could not provide any useful information about the chemical states of reduced samples.⁸ On the other hand, the EPR spectra showed a weak resonance signal at $g = 1.998$ for H₂-17%, which is known to be contributed by the presence of V_O²⁺ and Ti³⁺.^{40,41} No signal was observed with the pristine sample but an extremely low signal at the same position was found with the H₂-10%. We found that the photocatalytic activity of reduced anatase was proportional to the concentration of Ti³⁺,⁴² but our observation on reduced brookite was different (photocatalytic activity of H₂-17% was lower by ~60% than that of H₂-10%). Based on that, we concluded that V_O²⁺ and Ti³⁺ may form under reductive condition but are not main defect species responsible for the enhanced photocatalytic activity.

The photocatalytic activities were further evaluated for H₂ generation under UV light. Figure 11 compares the H₂

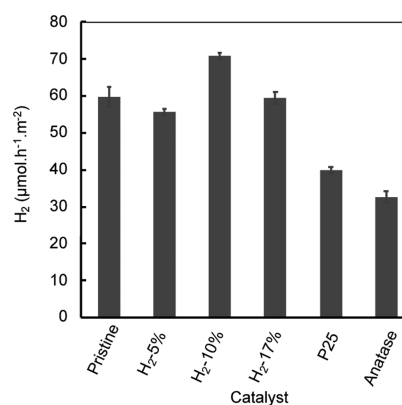


Figure 11. H₂ generation rates ($\mu\text{mol}\cdot\text{h}^{-1}\cdot\text{m}^{-2}$) of different TiO₂ samples under UV light. Values are normalized per a surface area basis.

generation rates of different TiO₂ samples: the activity of pristine was higher than that of anatase but lower than that of P25. It is known that the conduction band position of brookite locates deeper than that of anatase, benefitting its H₂ generation.⁵ The H₂-10% sample exhibited higher activity than the pristine sample and also much higher than P25. When normalized by surface areas (Table S2), the H₂ amount obtained from the H₂-10% sample was almost twice the amount produced by P25 and anatase (Figure S9). Similar to the catalytic activity for MB degradation, the H₂-17% sample showed rather deteriorated activity compared to the H₂-10% sample, further confirming that defects of brookite are susceptible to be altered by the different levels of reductive annealing atmospheres.

CONCLUSIONS

We investigated the defect equilibria and electronic structures of brookite and its effects on photocatalytic activities using DFT calculations and experiments. Brookite was found to have desirable defect-induced shallow levels that trap photoexcited electrons under mild reductive treatment. DFT calculations also suggested that the Ti_i⁴⁺ defect is the main defect to improve the photocatalytic activities of brookite. Concurrently, experimental generation of the Ti_i⁴⁺ defect was successfully carried out by H₂-assisted moderate reduction at 500 °C annealing conditions. Analysis by slow-scanned XRD, EXAFS, and EPR measurements indicated that lattice disorders in brookite increase as more reductive conditions are applied. Noteworthy is that Ti_i⁴⁺ and Ti_O⁴⁺ are identified as major defects rather than V_O²⁺ and Ti³⁺. This study informs the careful attention that must be paid in the heat treatment of brookite, especially when higher photocatalytic performance is required.

ASSOCIATED CONTENT

Supporting Information

The Supporting Information is available free of charge at <https://pubs.acs.org/doi/10.1021/acs.jpcc.0c02091>.

Digital images of TiO₂ powder; SEM and TEM/HR-TEM images; long-range and slow-scanned XRD; N₂

absorption and BET plots; XANES spectra; XPS spectra; tables of crystal properties, and particle structures (PDF)

AUTHOR INFORMATION

Corresponding Authors

Heechea Choi – Theoretical Materials & Chemistry Group, Institute of Inorganic Chemistry, University of Cologne, 50939 Cologne, Germany; orcid.org/0000-0002-9390-6607; Email: h.choi@uni-koeln.de

So-Hye Cho – Materials Architecturing Research Center, Korea Institute of Science and Technology (KIST), Seoul 02792, Korea; Division of Nano & Information Technology, KIST School, Korea University of Science and Technology, Daejeon 34113, Korea; orcid.org/0000-0001-9707-8629; Email: sohyec@kist.re.kr

Tae-seup Song – Department of Energy Engineering, Hanyang University, Seoul 04763, Korea; orcid.org/0000-0002-1174-334X; Email: tssong@hanyang.ac.kr

Authors

Sovann Khan – International Photocatalysis Research Center, Tokyo University of Science, Noda-shi, Chiba-ken 278-8510, Japan

Minyeong Je – Theoretical Materials & Chemistry Group, Institute of Inorganic Chemistry, University of Cologne, 50939 Cologne, Germany

Donghun Kim – Computational Science Research Center, Korea Institute of Science and Technology (KIST), Seoul 02792, Korea; orcid.org/0000-0003-0326-5381

Seungwoo Lee – Department of Energy Engineering, Hanyang University, Seoul 04763, Korea

Complete contact information is available at: <https://pubs.acs.org/10.1021/acs.jpcc.0c02091>

Author Contributions

H.C. and S.K. contributed for conceptualization, development of methodology, materials analysis, and writing-original-draft preparation. M.J. and D.K. contributed for theoretical calculations. S.L. carried out materials synthesis and analysis. S.-H.C. and T.S. contributed for funding acquisition conceptualization; supervision of experiments and calculations; and writing, reviewing, and editing.

Notes

The authors declare no competing financial interest.

ACKNOWLEDGMENTS

The EPR was analyzed at Korea Basic Science Institute (KBSI). XANES and EXAFS were obtained from the Advanced Analysis Center at the Korea Institute of Science and Technology (KIST-AAC). S.-H.C. acknowledges the financial support provided by the Korea Institute of Science and Technology Institutional projects (grant no. 2E29250). This work was supported by “Human Resources Program in Energy Technology” of the Korea Institute of Energy Technology Evaluation and Planning (KETEP), granted financial resource from the Ministry of Trade, Industry & Energy, Republic of Korea (no. 20194010201890). H.C. acknowledges the financial support of the Federal Ministry of Education and Research (BMBF) under the “Make Our Planet Great Again—German Research Initiative” (MOPGA-GRI; 57429784) implemented by the German Academic Exchange Service: Deutscher Akademischer Austauschdienst (DAAD).

REFERENCES

- (1) Chen, X.; Liu, L.; Yu, P. Y.; Mao, S. S. Increasing Solar Absorption for Photocatalysis with Black Hydrogenated Titanium Dioxide Nanocrystals. *Sci* **2011**, *331*, 746–750.
- (2) Choi, H.; Shin, D.; Yeo, B. C.; Song, T.; Han, S. S.; Park, N.; Kim, S. Simultaneously Controllable Doping Sites and the Activity of A W–N Codoped TiO₂ Photocatalyst. *ACS Catal.* **2016**, *6*, 2745–2753.
- (3) Li, Z.; Cong, S.; Xu, Y. Brookite vs Anatase TiO₂ in the Photocatalytic Activity for Organic Degradation in Water. *ACS Catal.* **2014**, *4*, 3273–3280.
- (4) Singh, S. C.; Swarnkar, R. K.; Gopal, R. Synthesis of Titanium Dioxide Nanomaterial by Pulsed Laser Ablation in Water. *J. Nanosci. Nanotechnol.* **2009**, *9*, 5367–5371.
- (5) Di Paola, A.; Bellardita, M.; Palmisano, L. Brookite, the Least Known TiO₂ Photocatalyst. *Catal* **2013**, *3*, 36–73.
- (6) Liu, L.; Peter, Y. Y.; Chen, X.; Mao, S. S.; Shen, D. Hydrogenation and Disorder in Engineered Black TiO₂. *Phys. Rev. Lett.* **2013**, *111*, 065505.
- (7) Khan, S.; Cho, H.; Kim, D.; Han, S. S.; Lee, K. H.; Cho, S.-H.; Song, T.; Choi, H. Defect Engineering Toward Strong Photocatalysis of Nb-doped Anatase TiO₂: Computational Predictions and Experimental Verifications. *Appl. Catal., B* **2017**, *206*, 520–530.
- (8) Lee, J.; Li, Z.; Zhu, L.; Xie, S.; Cui, X. Ti³⁺ Self-Doped TiO₂ via Facile Catalytic Reduction Over Al(acac)₃ with Enhanced Photoelectrochemical and Photocatalytic Activities. *Appl. Catal., B* **2018**, *224*, 715–724.
- (9) Choi, H.; Cho, S. H.; Khan, S.; Lee, K.-R.; Kim, S. Roles of an Oxygen Frenkel Pair in the Photoluminescence of Bi³⁺-doped Y₂O₃: Computational Predictions and Experimental Verifications. *J. Mater. Chem. C* **2014**, *2*, 6017–6024.
- (10) Janotti, A.; Varley, J.; Rinke, P.; Umezawa, N.; Kresse, G.; Van de Walle, C. Hybrid Functional Studies of the Oxygen Vacancy in TiO₂. *Phys. Rev. B: Condens. Matter Mater. Phys.* **2010**, *81*, 085212.
- (11) Ihm, J.; Zunger, A.; Cohen, M. L. Momentum-space formalism for the total energy of solids. *J. Phys. C: Solid State Phys.* **1979**, *12*, 4409–4422.
- (12) Choi, H.; Song, J. D.; Lee, K.-R.; Kim, S. Correlated Visible-Light Absorption and Intrinsic Magnetism of SrTiO₃ Due to Oxygen Deficiency: Bulk or Surface Effect? *Inorg. Chem.* **2015**, *54*, 3759–3765.
- (13) Freysoldt, C.; Grabowski, B.; Hickel, T.; Neugebauer, J.; Kresse, G.; Janotti, A.; Van de Walle, C. G. First-Principles Calculations for Point Defects in Solids. *Rev. Mod. Phys.* **2014**, *86*, 253.
- (14) Naldoni, A.; Allieta, M.; Santangelo, S.; Marelli, M.; Fabbri, F.; Cappelli, S.; Bianchi, C. L.; Psaro, R.; Dal Santo, V. Effect of Nature and Location of Defects on Bandgap Narrowing in Black TiO₂ Nanoparticles. *J. Am. Chem. Soc.* **2012**, *134*, 7600–7603.
- (15) Heyd, J.; Scuseria, G. E.; Ernzerhof, M. Hybrid Functionals Based on a Screened Coulomb Potential. *J. Chem. Phys.* **2003**, *118*, 8207–8215.
- (16) Perdew, J. P.; Burke, K.; Ernzerhof, M. Perdew, Burke, and Ernzerhof Reply. *Phys. Rev. Lett.* **1998**, *80*, 891.
- (17) Perdew, J. P.; Burke, K.; Ernzerhof, M. Generalized Gradient Approximation Made Simple. *Phys. Rev. Lett.* **1996**, *77*, 3865.
- (18) Kresse, G.; Hafner, J. Ab initio molecular dynamics for liquid metals. *Phys. Rev. B: Condens. Matter Mater. Phys.* **1993**, *47*, 558.
- (19) Reuter, K.; Scheffler, M. Composition, Structure, and Stability of RuO₂ (110) as a Function of Oxygen Pressure. *Phys. Rev. B* **2001**, *65*, 035406.
- (20) Tian, M.; Liu, C.; Ge, J.; Geohegan, D.; Duscher, G.; Eres, G. Recent Progress in Characterization of the Core-Shell Structure of Black Titania. *J. Mater. Res.* **2019**, *34*, 1138–1153.
- (21) Van de Walle, C. G.; Neugebauer, J. First-Principles Calculations for Defects and Impurities: Applications to III-Nitrides. *J. Appl. Phys.* **2004**, *95*, 3851–3879.
- (22) Setvin, M.; Franchini, C.; Hao, X.; Schmid, M.; Janotti, A.; Kaltak, M.; Van de Walle, C. G.; Kresse, G.; Diebold, U. Direct View

at Excess Electrons in TiO₂ Rutile and Anatase. *Phys. Rev. Lett.* **2014**, *113*, 086402.

(23) Choi, H.; Khan, S.; Choi, J.; Dinh, D. T. T.; Lee, S. Y.; Paik, U.; Cho, S.-H.; Kim, S. Synergetic Control of Band Gap and Structural Transformation for Optimizing TiO₂ Photocatalysts. *Appl. Catal., B* **2017**, *210*, 513–521.

(24) Chen, X.; Liu, L.; Huang, F. Black Titanium Dioxide (TiO₂) Nanomaterials. *Chem. Soc. Rev.* **2015**, *44*, 1861–1885.

(25) Noyes, W. A., Jr. The Reaction between Nitrogen and Hydrogen in the Presence of Mercury Vapor and the Resonance Radiation of Mercury. *J. Am. Chem. Soc.* **1930**, *52*, 2418–2419.

(26) Yu, J.; Qi, L.; Jaroniec, M. Hydrogen Production by Photocatalytic Water Splitting over Pt/TiO₂ Nanosheets with Exposed (001) Facets. *J. Phys. Chem. C* **2010**, *114*, 13118–13125.

(27) Kim, D.; Yeo, B. C.; Shin, D.; Choi, H.; Kim, S.; Park, N.; Han, S. S. Dissimilar Anisotropy of Electron versus Hole Bulk Transport in Anatase TiO₂: Implications for Photocatalysis. *Phys. Rev. B: Condens. Matter Mater. Phys.* **2017**, *95*, 045209.

(28) Dudarev, S. L.; Botton, G. A.; Savrasov, S. Y.; Humphreys, C. J.; Sutton, A. P.; Sutton, A. P. Electron-energy-loss spectra and the structural stability of nickel oxide: An LSDA+U study. *Phys. Rev. B: Condens. Matter Mater. Phys.* **1998**, *57*, 1505.

(29) Aaron Deskins, N.; Dupuis, M. Electron Transport via Polaron Hopping in Bulk TiO₂: A Density Functional Theory Characterization. *Phys. Rev. B: Condens. Matter Mater. Phys.* **2007**, *75*, 195212.

(30) De Lile, J. R.; Kang, S. G.; Son, Y.-A.; Lee, S. G. Investigating Polaron Formation in Anatase and Brookite TiO₂ by Density Functional Theory with Hybrid-Functional and DFT + U Methods. *ACS Omega* **2019**, *4*, 8056–8064.

(31) Štengl, V.; Kralova, D. Photoactivity of Brookite-Rutile TiO₂ Nanocrystalline Mixtures Obtained by Heat Treatment of Hydrothermally Prepared Brookite. *Mater. Chem. Phys.* **2011**, *129*, 794–801.

(32) Hall, R. N. Electron-Hole Recombination in Germanium. *Phys. Rev.* **1952**, *87*, 387.

(33) Shockley, W.; Read, W. T., Jr. Statistics of The Recombinations of Holes and Electrons. *Phys. Rev.* **1952**, *87*, 835.

(34) Vequizo, J. J. M.; Matsunaga, H.; Ishiku, T.; Kamimura, S.; Ohno, T.; Yamakata, A. Trapping-Induced Enhancement of Photocatalytic Activity on Brookite TiO₂ Powders: Comparison with Anatase and Rutile TiO₂ Powders. *ACS Catal.* **2017**, *7*, 2644–2651.

(35) Song, T.; Paik, U. TiO₂ as an Active or Supplemental Material for Lithium Batteries. *J. Mater. Chem. A* **2016**, *4*, 14–31.

(36) Bakardjieva, S.; Stengl, V.; Szatmary, L.; Subrt, J.; Lukac, J.; Murafa, N.; Niznansky, D.; Cizek, K.; Jirkovsky, J.; Petrova, N. Transformation of Brookite-Type TiO₂ Nanocrystals to Rutile: Correlation Between Microstructure and Photoactivity. *J. Mater. Chem.* **2006**, *16*, 1709–1716.

(37) Liu, X.; Zhu, G.; Wang, X.; Yuan, X.; Lin, T.; Huang, F. Progress in Black Titania: A New Material for Advanced Photocatalysis. *Adv. Energy Mater.* **2016**, *6*, 1600452.

(38) Justicia, I.; Ordejón, P.; Canto, G.; Mozos, J. L.; Fraxedas, J.; Battiston, G. A.; Gerbasi, R.; Figueras, A. Designed Self-Doped Titanium Oxide Thin Films for Efficient Visible-Light Photocatalysis. *Adv. Mater.* **2002**, *14*, 1399–1402.

(39) Schneider, J.; Matsuoka, M.; Takeuchi, M.; Zhang, J.; Horiuchi, Y.; Anpo, M.; Bahnemann, D. W. Understanding TiO₂ Photocatalysis: Mechanisms and Materials. *Chem. Rev.* **2014**, *114*, 9919–9986.

(40) Xing, M.; Zhang, J.; Chen, F.; Tian, B. An Economic Method to Prepare Vacuum Activated Photocatalysts With High Photo-Activities and Photosensitivities. *Chem. Commun.* **2011**, *47*, 4947–4949.

(41) Fang, W.; Xing, M.; Zhang, J. A New Approach to Prepare Ti³⁺ Self-Doped TiO₂ via NaBH₄ Reduction and Hydrochloric Acid Treatment. *Appl. Catal., B* **2014**, *160–161*, 240–246.

(42) Xing, M.; Fang, W.; Nasir, M.; Ma, Y.; Zhang, J.; Anpo, M. Self-doped Ti³⁺-Enhanced TiO₂ Nanoparticles with a High-Performance Photocatalysis. *J. Catal.* **2013**, *297*, 236–243.